The critical stable length in wrinkles of two-dimensional materials

AUTHOR NAMES:

Fangyuan Zheng[1,2], Lok Wing Wong[1,2], Quoc Huy Thi[3,4], Qingming Deng[5]*, Thuc Hue Ly[3,4]* and Jiong Zhao[1,2]*

AUTHOR ADDRESS:

[1] Department of Applied Physics, The Hong Kong Polytechnic University, Kowloon, Hong Kong, China.

[2] The Hong Kong Polytechnic University Shenzhen Research Institute, Shenzhen, China.

[3] Department of Chemistry and Center of Super-Diamond & Advanced Films (COSDAF), City University of Hong Kong, Kowloon, Hong Kong, China.

[4] City University of Hong Kong Shenzhen Research Institute, Shenzhen, China.

[5] Physics department and Jiangsu Key Laboratory for Chemistry of Low-Dimensional Materials, Huaiyin Normal University, Huaian 223300, China.

KEYWORDS: wrinkle, 2D materials, critical length, thermal annealing, *in situ* transmission electron microscopy

Abstract:

The emergent two-dimensional (2D) materials are atomically thin and ultra-flexible, promising for a variety of miniaturized, high-performance and flexible devices in applications. On one hand, the ultrahigh flexibility causes problems—the prevalent wrinkles in 2D materials may undermine the ideal properties and create barriers in fabrication, processing and quality control of materials. On the other hand, in some cases the wrinkles are used for the architecturing of surface texture and the modulation of physical/chemical properties. Therefore, a thorough understanding in the mechanism and stability of wrinkles is highly needed. Herein, we report a critical length for stabilizing the wrinkles in 2D materials, observed in the wrinkling and dewrinkling processes upon thermal annealing as well as by our *in situ* TEM manipulations on individual wrinkles, which directly capture the evolving wrinkles with variable lengths. The experiments, mechanical modelling, and the density functional theory (DFT) simulations consistently reveal that a minimum critical length is requested for stabilizing the wrinkles in 2D materials. Short wrinkles are unstable and removable by thermal annealing, whilst long wrinkles are self-stabilized by van der Waals (vdW) interactions. It additionally confirms the pronounced frictional effects in long wrinkles during the dynamical movement or sliding.

Main text:

Wrinkles widely exist in the natural and artificial membranes, they can store considerable elastic (bending) energy in case suitable boundary conditions are imposed. Normally, wrinkles are in unstable structures if the boundaries or fixtures are allowed to relax[1]. The mechanical description of wrinkles is generally based on the continuum theory[2,3]. For the smaller bending rigidity of thinner membranes, winkling is more easily triggered. However, for the membranes with thickness down to atomic-scale, influences from the significant surface interactions and the breakdown of continuum mechanics in atomic or nano-sized objects[4] create substantial difficulties in the mechanical analysis. Contrary to the unstable nature of the

conventional wrinkles, the key finding of this work is the stable wrinkle structures revealed in the two-dimensional (2D) materials, caused by the van der Waals (vdW) interactions, which means an energy barrier needs to be overcome before wrinkling and dewrinkling. Furthermore, the minimum length (or height) for stabilizing the wrinkles of 2D materials are determined both experimentally and theoretically.

The emergent ultra-thin atomic-layered membranes, namely, 2D materials[5,6], such as graphene and MoS_2 mono-atomic layer[7-9], were discovered and extensively studied in recent years. Their high flexibility nature is well known. Specifically, nanotubes with nm-diameters can be formed by 2D membranes[10,11], folded[12] or creased[13] 2D structures have been observed as well. Meanwhile, wrinkles are frequently observed with compressive or bending stress on 2D materials, particularly with respect to the substrates[14]. Even without intention, wrinkles can be formed during the fabrication and especially the post-processing/transferring of 2D materials[15], suggesting the undermined performances in applications. The mechanical, electrical/electronic and thermal properties can all be potentially influenced by wrinkles[16]. In another aspect, wrinkles, particularly with designable textured architectures, play important roles in stretchable and flexible devices[17] as well as in nano-fluidic devices[18], which greatly enrich the application areas of 2D materials.

Wrinkles in 2D materials have been recently studied by atomic force microscopy (AFM)[19], scanning tunnelling microscopy (STM)[20] and transmission electron microscopy (TEM)[21], their structures as well as the modulated electronic band structures which are quite different from the flat zones have been reported[22]. However, so far the mechanical stability and the dynamical behaviour of individual wrinkles have not been addressed, especially by direct *in situ* experiments. Although the flexural properties and wrinkle structures of 2D materials can be assessed by theoretical approaches such as density functional theory (DFT)[23], in contrast to the accessible basal-plane tensile tests on 2D materials[24], at present, the continuous flexural properties of 2D materials and the quantitative descriptions are still unknown. Particularly, some

in situ transmission electron microscopy (TEM) experiments have allowed the dynamic observations of rippling[25] or exfoliation[26] processes of 2D materials, however, the dynamics of the wrinkle structures dependent on the lengths are unexplored, in part due to the difficulties regarding the loading fixture and the atomic-scale manipulation of 2D membranes. Standard flexural testing applies a two- to four-point fixture on the sample[27,28], and the elastic modulus of bending, flexural strength and flexural stress-strain responses can be retrieved[29-32]. However, all the classical flexural methods apparently fail in cases of ultra-thin or ultra-flexible membranes due to the infinitesimal bending rigidity in membranes, which are not stable or self-standing during external perturbations, such as gravity or thermal fluctuations[33-36]. Indeed, similar to polymer molecules, the persistence length of atomic-thick 2D materials falls into the nanometre (nm) scale[37, 38]. Therefore, here we apply the atomic force microscopy (AFM) and direct *in situ* TEM approaches to understand the wrinkle dynamics and stability under thermal and mechanical perturbations.

In the first experiment, the thermal stability of wrinkles in monolayer graphene is examined (Figure 1a). The large area graphene samples used are grown by chemical vapor deposition (CVD) method and transferred onto the SiO_2/Si wafers by a poly (methyl methacrylate) (PMMA) transfer process (see methods)[39], which has been routinely used in the processing for the 2D materials. As usual, the morphology of the monolayer graphene on SiO_2 is found quite rough in nanoscale. Figure 1b shows a typical AFM topographic image for the transferred monolayer graphene sample. The crossed parallel stripes are the wrinkle patterns induced naturally during PMMA transfer. The spikes on the AFM line profile (Figure 1b) correspond to the position and height of the individual wrinkles. The height of wrinkles spans from 0.1 nm to 1.7 nm with a sample roughness of ca. 0.7 nm. After thermal annealing at 200ºC for 8 hours, the same sample position is checked using AFM (Figure 1c). The original big wrinkles (height over 1.5 nm) are unaffected by the thermal annealing, while the small wrinkles are mostly eliminated or combined with big wrinkles. Figure 1a shows the schematic diagram of the shape of wrinkles before and after annealing

and the mechanisms will be discussed in following paragraphs. The AFM experiments clearly demonstrate that thermal annealing is an effective way to remove small wrinkles. The critical height of the stable wrinkles in monolayer graphene against thermal activation can be explicitly investigated via the following *in situ* TEM experiments.

In our second *in situ* transmission electron microscopy (TEM) test, multilayer graphene samples are mechanically exfoliated from highly ordered pyrolytic graphite (HOPG) crystals using Scotch tape[8]. The selected area electron diffraction (SAED) pattern of multilayer graphene exhibits good crystallinity in the samples and facilitates crystal direction identification in the flakes (Figure S1). The *in situ* TEM manipulation holder (Nanofactory^{TM}) with a precision better than 0.1 nm in three-dimensional (3D) space is employed (Figure 2a). In the first step, an electrochemical etched W tip is controlled by the piezo-manipulator and is firmly pressed on the top surface of the multilayer (layer number >10, counted at edge) graphene (Figure 2b, c). Then, the W tip (less than 5 nm by 5 nm) intentionally scratches along the graphene surface until a one-nm crack emerges on the top layer of graphene. Afterwards, the W tip is laterally moved on the flake surface for further tearing of the top graphene layer until it is gradually exfoliated from the multilayer underneath (Figure 2b). The monolayer thickness of the exfoliated layer is confirmed directly at the flake edge, and no additional exfoliation in the separated top layer can be seen with further manipulation. The initial crack edge in the top layer is adsorbed/connected to the W tip. Following the initial exfoliation, sequential wrinkles are spontaneously formed in the top monolayer (Figure 2b) by vdW interactions. The wrinkle direction is along the zigzag direction, as confirmed by SAED. Owing to the three-fold symmetry of graphene, the bending properties can be considered almost isotropic in the basal plane[40].

After several wrinkles are shaped, the movement of the W tip is reversed in the opposite direction, namely, the recovery direction (Figure 2d, e). A straight stripe with sharper contrast starts to replace the previous obscured wrinkled images (Figure 2f, red triangle marks). This observation agrees with our following analysis, indicating that a self-standing wrinkle with a regular shape between two vdW contacts is naturally formed. Afterwards, the W tip is further moved along the recovery direction, thus resulting in the gradual shortening of the total wrinkle length (l) and height, manifested by a decrease in the stripe contrast (Figure 2f). Next, a quick drop in the wrinkle image contrast and wrinkle length led by the continuous movement of the W tip (last snapshot in Figure 2f) shows the entire recovery of the wrinkle. Interestingly, after recovery, the image contrast in the exfoliated top layer and the adjacent perfect part are almost the same, implying that the wrinkle has perfectly recovered. Notably, other wrinkles with the W tip demonstrate no appreciable change in morphology during manipulation.

After the first recovery is completed, the W tip is further moved along the recovery direction. Since a few more wrinkles are reserved during the tearing process, a total of seven similar recovery processes are completed in this experiment (Figure 2g~2i shows three of them). After the last few recoveries (Figure 2h, i), some short wrinkles remain close to the cracks/edges due to a slight rotation in the top layer with respect to the multilayer underneath. In addition, the recovery mainly occurs when the sliding contact area (area denoted by x in Figure 2d) is small; once the contact area increases after sliding, some remaining wrinkles can be "locked" due to high frictional forces.

The observed continuous manipulation can be quantified via measurements on the physical positions of the wrinkles, including the wrinkles due to on-going tests and their adjacent wrinkles. For the convenience of analysis, here we define the total length of a wrinkle (denoted as l) as the integrated curved length excluding the underlying flat length, which can be determined by the variation in the positions (prior to/after recovery) of the adjacent wrinkles (Figure 2d, also see Figure S2). During the manipulations,

based on our measurements, the lengths of all the wrinkles are stepwise shortened (the last few steps for each wrinkle are shown in Figure 3a). The corresponding distances between the last two wrinkles (Figure 2d), the same as the area of the sliding contact zone (x), are recorded as well. Although the continuous movement of the W tip is piezo-controlled with a constant speed and precision as high as 0.1 nm, a stick-slip behaviour in the sliding is observed. The lattice-commensurate vdW contact between the two vdW bearings introduces a frictional force (f), which is proportional to the contact area x[41]. Thus, the distance or step of each "stick-slip" move (Δl) can be expressed as

$$f = k\Delta l = \mu x, \quad (1)$$

where k is the (lateral) force constant of the W tip and μ is the friction coefficient between the vdW layers. The above linear dependence of each stick-slip movement on the contact area coincides with our experimental results (Figure 3b). Each x and l are statistically measured from multiple positions on the wrinkles. Moreover, by excluding the distance of the last stick-slip frictional movement, the critical lengths (l_c) for the wrinkles before the last flattening step (drop to zero of l) are shown in Figure 3c (the distances in the last move of the W tip are subtracted according to eq. 1 and Figure 3b). The results are surprisingly close to a common threshold length of ca. 4.0 nm, which is due to the specular mechanical responses in the top graphene layer, as elaborated below.

A linear continuum mechanics model[42] can be applied and verified on monolayer graphene[43]. The differences between graphene on SiO_2 in our first experiment and graphene on multilayer graphene in the second experiment is just the different vdW interactions with the substrates (Figure 3d). The shapes of the wrinkles with minimized energy at different total lengths (l) are exhibited in Figure 3e. For the bending rigidity and the vdW interlayer energy of graphene, widely accepted experimental values are adopted[44,45]. A clear transition from the "clip" shape (Figure 3e, state 1 to state 2, also called type 3 shape, see Figure S3) to the "bump" shape (state 3 to state 6, also called type 2 shape) is denoted. A transition occurs near the wrinkle length (l) of 4.1~4.3 nm for the multilayer graphene case (l_c=3.9 nm for graphene-SiO_2 case).

The strain forces restored in the wrinkles are calculated and presented in the supplementary materials. In long wrinkle cases, due to vdW adsorption, the clipped wrinkles (type 3) are stabilized and no strain is applied to the two vdW contact bearings; however, after the critical transition (state 2 to state 3), considerable shear strain is set in the contact bearings due to the bending strains in the top layer. Thus, the wrinkles become unstable and are liable to be flattened if the frictional vdW forces are insufficient to balance the bending strains. Comparing the results of modelling with our AFM and *in situ* TEM experiments on the critical height/length of the wrinkles, the height by AFM (critical height ~1.5 nm) has larger error with the 2.3 nm by modelling, possibly resulted from the larger friction at the graphene-SiO_2 interface, while the *in situ* TEM results (l_c~4.0 nm) coincides well with the results (l_c=4.1~4.3) of modelling.

To further understand and validate the wrinkling behaviour, the structural optimizations of the wrinkles are carried out by the self-consistent charge density functional tight binding (SCC-DFTB) method[46]. The longest length of the wrinkles is set from approximately 6 nm to accommodate the clipped wrinkles (Figure 3f, states 1 and 2) until the shortest single unit cell (l=0.24 nm) wrinkle (Figure 3f, state 6), which actually becomes an edge dislocation. The short wrinkles can indeed be considered as a dislocation or a ripplocation in 2D[47]. The relaxed wrinkled structures in monolayer graphene are in agreement with the previous continuous mechanics models (Figure 3e, f). According to the continuous mechanics model and DFTB simulation, the transition between the clip state to the bump state (Figure 3f, critical transition from state 2 to state 3) occurs at a wrinkle length of approximately 3.8 nm. Therefore, the experimental results (4.0 nm) again largely agree with the DFTB results (3.8 nm) for the critical transition point of "unclipping" and strain release.

Except for the bended shapes and total wrinkle lengths, which are in equilibrium, the dynamic positions of wrinkles under testing exhibit an interesting dependence on the wrinkle lengths as well. The displacement of the wrinkles (Δx) versus the total wrinkle length change (Δl) at different wrinkle lengths (l) in

our experiments is shown in Figure 4a. With the pulling forces (see schematic Figure 4b) by the W tip, the wrinkles slowly move along the recovery direction. The pulling effect (defined as $\Delta x/\Delta l$) on the wrinkle decreases with reduced wrinkle lengths. Short wrinkles have Δx=0 in recovery due to the direct momentum transfer to the whole wrinkle and frictionless dynamics in the clipped areas (Figure 4b). In contrast, for long clipped wrinkles, the recovery process tends to cause no relative sliding between the two clipped sides of the wrinkles (Figure 4b). Therefore, the wrinkles in the long length limit will have the maximum $\Delta x/\Delta l$ equal to 1/2 (Figure 4b), which is consistent with our experimental observations (Figure 4a). The *in situ* monitoring of the entire wrinkling and dewrinkling process provides important additional insights. To further improve the test setting, the manipulating tip with a larger force constant can be sought, which means that the stick-slip steps will be finer; hence, the dynamics close to the critical threshold of state transition during the entire testing can be more clearly unravelled.

In conclusion, the experiments here directly exhibit the wrinkling and dewrinkling process of graphene, and the concepts here can be readily generalized to other vdW layered 2D materials. Wrinkles can either facilitate or deteriorate the performances, depending on the way they are treated. The 2D materials community is always keen to the flatness and uniformity, but also enthusiastic for the flexibility. The obtained critical lengths for wrinkling/dewrinkling here is expected to have profound impacts in the future development of flexible electronic/optoelectronic devices, nanoelectromechanical systems (NEMS) and other related fields.

Methods

Sample preparation and annealing: Graphene was synthesized on a 75 μm thick copper foil (Goodfellow, England) using tube furnace (Nabertherm, Germany) in atmospheric pressure. The temperature in the tube was elevated to the growth temperature within 30 minutes, and samples were annealed at the growth

temperature for 2 hours with flow gases of 50 sccm H2 and 50 sccm Ar. Monolayer graphene was synthesized with a flow of 50 sccm H2, 10 sccm CH4 (1% in Ar) and 1000 sccm Ar for 45 minutes. The sample was then cooled to room temperature while maintaining the 1000 sccm Ar flow. After synthesis, Poly(methyl methacrylate) (PMMA) was spin-coated onto the graphene-grown Cu foil at 800 rpm for 10 seconds and then 3000 rpm for 1 minute. Copper etchant (Aldrich 667528) was used to dissolve the underlying copper. The PMMA-coated graphene was transferred onto the SiO_2/Si substrate. This sample was dried in a dry oven at 65 °C before PMMA was removed with acetone. Further, the graphene/SiO_2/Si substrate was put back to the tube furnace then annealed at 200 °C for 8 hours. Low vacuum of 2×10^{-2} mbar was maintained from beginning until cooling to room temperature. Before and after annealing, surface of transferred graphene was investigated by atomic force microscope (AFM). The topography and phase images were obtained using the AFM5300 system (Hitachi, Japan) in tapping mode. A NSC30-type silicon tip (Tipsnano, Estonia) with an approximately 10-nm tip curvature radius was used. The multilayer graphene membranes were produced by mechanical exfoliation from bulk materials using adhesive tapes. Bulk graphite (ZYA Grade, provided by 2D Semiconductors Inc., USA) were mechanically exfoliated into several layers on Scotch tape. Then, graphene monolayers with good quality but small flakes could be dry-transferred on a TEM grid directly by the heat release tape method with clean surfaces. The grids are then fixed on an *in situ* TEM manipulation holder (Nanofactory^{TM}) fitted in the JEOL 2100F TEM, while an electrochemically etched tungsten (W) tip is installed on the counter position, which can be finely piezo-controlled with a precision better than 0.1 nm in three-dimensional (3D) space. The W tips used for the *in situ* TEM manipulator were made by electrochemical corrosion with a solution of 1 mol/L NaOH at a 2~3 V bias.

TEM characterizations and analysis: The TEM images and videos were collected on a JEOL 2100F transmission electron microscope under an accelerating voltage of 200 kV with a Nanofactory^{TM} STM-TEM holder. The bright-field TEM imaging in our *in situ* experiments was acquired via a 0.5 s exposure time and electron dose lower than 0.1 A/cm^{-2}. The position of each wrinkle and corresponding x and l were measured from five different spots on the wrinkles and averaged.

DFTB calculations: The calculations in this study were performed using the DFTB+ code[48]. The structural optimizations and energies of graphene wrinkles were evaluated by 41 SCC approximations of the DFTB method, which was based on a second-order expansion of the DFT total energy with respect to charge density fluctuations. The carbon-carbon interaction was described by the mio-0-1 set of parameters, and the dispersion corrections for the nonbonding van der Waals interaction were implemented via the Lennard Jones type model[49]. Two graphene layer slabs of size 214×2.47 Å (396-448 carbon atoms) and 350 Å of vacuum were used to simulate the bending processes of the wrinkles, and the Brillouin zone was sampled with a 2×8×1 Monkhorst-Pack grid of points.

Continuum mechanics modelling: The bending moment at the start point of curvature is balanced by

$$M - M_R + fx = 0,$$

where M, M_R, and f are the bending moment at cut, the bending moment at the contact edge and the friction force between the top layer and the multilayer substrate, respectively. The expression of M is given by

$$M = D\frac{d\phi}{ds},$$

where D is the bending stiffness, which can be expressed by $D = \frac{Et^3}{12(1-v^2)}$; E is Young's modulus; v is Poisson's ratio and t is the effective thickness of the material. From the bending curvature of the sheet, we know $dx/ds = sin\,\phi$, $dy/ds = -cos\,\phi$. Deriving from the above equations, we have

$$\frac{d^2\phi}{ds^2} = -\frac{f}{D}\cos\phi,$$

Define $\gamma \equiv \sqrt{\frac{W_{ad}}{f}}$, $\Phi'(0) = \sqrt{\frac{W_{ad}}{D}}$, where W_{ad} is the adhesion energy between two vdW layers, which can be regarded as the boundary condition since it balances the adhesion energy and strain energy. Given a value of γ, the curvature of the sheet under a certain value can be determined and fitted with experiments,

which represents the shape of the graphene wrinkles. The corresponding total energy and friction force can be calculated. For the critical transition between state 2 and state 3, as depicted in Figure 3e, the energy of the two states should be the same within the margin of error by changing one unit cell length of graphene, i.e., 0.24 nm. We find that the transition occurs when the length of the wrinkle reaches 4.05 nm. In addition to the flexural texting on graphite substrate, we also simulate the flexural on SiO_2 substrate. The bending curvatures is shown in Figure 3d, e. The main difference between graphite and SiO_2 as the substrate is the adhesion energy of graphene with them, which makes slight change in boundary conditions in the model.

Corresponding Author

qingmingdeng@gmail.com (Q.D.), thuchly@cityu.edu.hk(T.H.L.), jiongzhao@polyu.edu.hk (J.Z.)

Notes

The authors declare no financial or non-financial conflicts of interest.

ACKNOWLEDGMENT

This work was supported by Hong Kong Research Grant Council Early Career Scheme (Project no.25301018,), the Hong Kong Research Grant Council under the ECS CityU (9048127), City University of Hong Kong (Project No. 9610387), National Science Foundation of China (51872248, 21703076), Natural Science Foundation of Jiangsu Province of China (BK20170466), 333 High-level Talents Cultivating Project of Jiangsu Province (BRA2018341) and Shenzhen Science and Technology Innovation Commission (Project no. JCYJ20170818104717087).

REFERENCES

1. Rayleigh, L. *Theory of Sound Vol. 1*, **1945**, 396.
2. Cerda, E.; Ravi-Chandar, K.; Mahadevan, L. Thin films: wrinkling of an elastic sheet under tension. *Nature* **2002**, 419, 579-580.
3. Cerda, E.; Mahadevan, L. Geometry and Physics of Wrinkling. *Physical review letters* **2003**, 90, 074302.
4. Luan, B.; Robbins, M. O. The breakdown of continuum models for mechanical contacts. *Nature* **2005**, 435, 929.
5. Zhu, W.; Low, T.; Perebeinos, V.; Bol, A. A.; Zhu, Y.; Yan, H.; Avouris, P. Structure and electronic transport in graphene wrinkles. *Nano letters* **2012**, 12, 3431-3436.
6. Xu, M.; Liang, T.; Shi, M.; Chen, H. Graphene-Like Two-Dimensional Materials. *Chemical reviews* **2013**, 5, 3766-3798.
7. Butler, S. Z.; Hollen, S. M.; Cao, L.; Cui, Y.; Gupta, J. A.; Gutiérrez, H. R. Progress, challenges, and opportunities in two-dimensional materials beyond graphene. *ACS nano* **2013**, 4, 2898-2926.
8. Novoselov, K. S.; Geim, A. K.; Morozov, S. V.; Jiang, D.; Zhang, Y.; Dubonos, S. V.; Firsov, A. A. Electric field effect in atomically thin carbon films. *Science* **2004**, 306, 666-669.
9. Novoselov, K. S.; Fal, V. I.; Colombo, L.; Gellert, P. R.; Schwab, M. G.; Kim, K. A roadmap for graphene. *Nature* **2012**, 490, 192-200.
10. Mak, K. F.; Lee, C.; Hone, J.; Shan, J.; Heinz, T. F. Atomically thin MoS 2: a new direct-gap semiconductor. *Physical review letters* **2010**, 105, 136805.
11. Seifert, G.; Terrones, H.; Terrones, M.; Jungnickel, G.; Frauenheim, T. Structure and electronic properties of MoS2 nanotubes. *Physical Review Letters* **2000**, 85, 146.
12. Qin, L. C.; Zhao, X.; Hirahara, K.; Miyamoto, Y.; Ando, Y.; Iijima, S. Materials science: The smallest carbon nanotube. *Nature* **2000**, 408, 50.

13. Ortolani, L.; Cadelano, E.; Veronese, G. P.; Degli Esposti Boschi, C.; Snoeck, E.; Colombo, L.; Morandi, V. Folded graphene membranes: mapping curvature at the nanoscale. *Nano letters* **2012** 12, 5207-5212.

14. Cranford, S. W.; Buehler, M. J. Packing efficiency and accessible surface area of crumpled graphene. *Physical Review B* **2011**, 84, 205451.

15. Akinwande, D.; Brennan, C. J.; Bunch, J. S.; Egberts, P.; Felts, J. R.; Gao, H.; Liechti, K. M. A review on mechanics and mechanical properties of 2D materials—Graphene and beyond. *Extreme Mechanics Letters* **2017**, 13, 42-77.

16. Deng, S.; Berry, V. Wrinkled, rippled and crumpled graphene: an overview of formation mechanism, electronic properties, and applications. *Materials Today* **2016**, 19, 197-212.

17. Hu, H. W.; Haider, G.; Liao, Y. M.; Roy, P. K.; Ravindranath, R.; Chang, H. T.; Chen, Y. F. Wrinkled 2D materials: A versatile platform for low-threshold stretchable random lasers. *Advanced Materials* **2017**, 29, 1703549.

18. Park, S. M.; Huh, Y. S.; Craighead, H. G.; Erickson, D. A method for nanofluidic device prototyping using elastomeric collapse. *Proceedings of the National Academy of Sciences* **2009**, 106, 15549-15554.

19. Meng, L.; Su, Y.; Geng, D.; Yu, G.; Liu, Y.; Dou, R. F.; He, L. Hierarchy of graphene wrinkles induced by thermal strain engineering. *Applied Physics Letters* **2013**, 103, 251610.

20. Xu, P.; Neek-Amal, M.; Barber, S. D.; Schoelz, J. K.; Ackerman, M. L.; Thibado, P. M.; Peeters, F. M. Unusual ultra-low-frequency fluctuations in freestanding graphene. *Nature communications* **2014**, 5, 3720.

21. Meyer, J. C.; Geim, A. K.; Katsnelson, M. I.; Novoselov, K. S.; Booth, T. J.; Roth, S. The structure of suspended graphene sheets. *Nature* **2007**, 446, 60–63.

22. Pereira, V. M.; Neto, A. C.; Liang, H. Y.; Mahadevan, L. Geometry, mechanics, and electronics of singular structures and wrinkles in graphene. *Physical review letters* **2010**, 105, 156603.

23. Wei, Y.; Wang, B.; Wu, J.; Yang, R.; Dunn, M. L. Bending rigidity and Gaussian bending stiffness of single-layered graphene. *Nano letters* **2012**, 13, 26-30.

24. Lee, C.; Wei, X.; Kysar, J. W.; Hone, J. Measurement of the elastic properties and intrinsic strength of monolayer graphene. *Science* **2008**, 321, 385-388.

25. Ludacka, U.; Monazam, M. R. A.; Rentenberger, C.; Friedrich, M.; Stefanelli, U.; Meyer, J. C.; Kotakoski, J. In situ control of graphene ripples and strain in the electron microscope. *2D Materials and Applications* **2018**, 2, 25.

26. Tang, D. M.; Kvashnin, D. G.; Najmaei, S.; Bando, Y.; Kimoto, K.; Koskinen, P.; Golberg, D. Nanomechanical cleavage of molybdenum disulphide atomic layers. *Nature communications* **2014**, 5, 3631.

27. Landau, L.; Lifshitz, E. Theoretical Physics. Vol. 3. Continuum Mechanics. *Pergamon Press, Oxford* **1944**.

28. Mujika, F. On the difference between flexural moduli obtained by three-point and four-point bend-ing tests. *Polymer Testing* **2006**, 25, 214-220.

29. Boukhili, R.; Hubert, P.; Gauvin, R. Loading rate effect as a function of the span-to-depth ratio in three-point bend testing of unidirectional pultruded composites. *Composites* **1991**, 22, 39-45.

30. Quinn, G. D.; Sparenberg, B. T.; Koshy, P.; Ives, L. K.; Jahanmir, S.; Arola, D. D. Flexural strength of ceramic and glass rods. *Journal of Testing and Evaluation* **2009**, 37, 222-244.

31. Combes, S. A.; Daniel, T. L. Flexural stiffness in insect wings II. Spatial distribution and dynamic wing bending. *Journal of Experimental Biology* **2003**, 206, 2989-2997.

32. Yoo, D. Y.; Yoon, Y. S.; Banthia, N. Flexural response of steel-fiber-reinforced concrete beams: Effects of strength, fiber content, and strain-rate. *Cement and Concrete Composites* **2015**, 64, 84-92.

33. Castellanos-Gomez, A.; Singh, V.; van der Zant, H. S.; Steele, G. A. Mechanics of freely-suspended ultrathin layered materials. *Annalen der Physik* **2015**, 527, 27-44.

34. Huang, R., Stafford, C. M.; Vogt, B. D. Effect of surface properties on wrinkling of ultrathin films. *Journal of Aerospace Engineering* **2007**, 20, 38-44.

35. Bao, W.; Miao, F.; Chen, Z.; Zhang, H.; Jang, W.; Dames, C.; Lau, C. N. Controlled ripple texturing of suspended graphene and ultrathin graphite membranes. *Nature nanotechnology* **2009**, 4, 562-566.

36. Fournier, J. B.; Ajdari, A.; Peliti, L. Effective-area elasticity and tension of micromanipulated membranes. *Physical review letters* **2001**, 86, 4970.

37. Fasolino, A.; Los, J. H.; Katsnelson, M. I. Intrinsic ripples in graphene. *Nature materials* **2007**, 6, 858-861.

38. Xu, Z.; Buehler, M. J. Geometry controls conformation of graphene sheets: membranes, ribbons, and scrolls. *ACS nano* **2010**, 4, 3869-3876.

39. Gao, L.; Ni, G. X.; Liu, Y.; Liu, B.; Neto, A. H. C.; Loh, K. P. Face-to-face transfer of wafer-scale graphene films. *Nature* **2014**, 505, 190–194.

40. Lu, Q.; Arroyo, M.; Huang, R. Elastic bending modulus of monolayer graphene. *Journal of Phys-ics D: Applied Physics* **2009**, 42, 102002.

41. Enachescu, M.; Van den Oetelaar, R. J. A.; Carpick, R. W.; Ogletree, D. F.; Flipse, C. F. J.; Salm-eron, M. Observation of proportionality between friction and contact area at the nanometer scale. *Tribology Letters* **1999**, 7, 73.

42. Yakobson, B. I.; Brabec, C. J.; Bernholc, J. Nanomechanics of carbon tubes: instabilities beyond linear response. *Physical review letters* **1996**, 76, 2511.

43. Wang, C. Y.; Mylvaganam, K.; Zhang, L. C. Wrinkling of monolayer graphene: a study by molecular dynamics and continuum plate theory. *Physical Review B* **2009**, 80, 155445.

44. Zhao, J.; Deng, Q.; Ly, T. H.; Han, G. H.; Sandeep, G.; Rümmeli, M. H. Two-dimensional membrane as elastic shell with proof on the folds revealed by three-dimensional atomic mapping. *Nature communications* **2015**, 6, 8935.

45. Lu, Q.; Arroyo, M.; Huang, R. Elastic bending modulus of monolayer graphene. *Journal of Phys-ics D: Applied Physics* **2009**, 42, 102002.

46. Elstner, M.; Porezag, D.; Jungnickel, G.; Elsner, J.; Haugk, M.; Frauenheim, T.; Seifert, G. Self-consistent-charge density-functional tight-binding method for simulations of complex materials properties. *Physical Review B* **1998**, 58, 7260.

47. Kushima, A.; Qian, X.; Zhao, P.; Zhang, S.; Li, J. Ripplocations in van der Waals layers. *Nano letters* **2015**, 15, 1302-1308.

48. Aradi, B.; Hourahine, B.; Frauenheim, T. DFTB+, a sparse matrix-based implementation of the DFTB method. *The Journal of Physical Chemistry A* **2007**, 111, 5678-568.

49. Rappé, A. K.; Casewit, C. J.; Colwell, K. S.; Goddard III, W. A.; Skiff, W. M. UFF, a full peri-odic table force field for molecular mechanics and molecular dynamics simulations. *Journal of the American chemical society* **1992**, 114, 10024-10035.

Figures

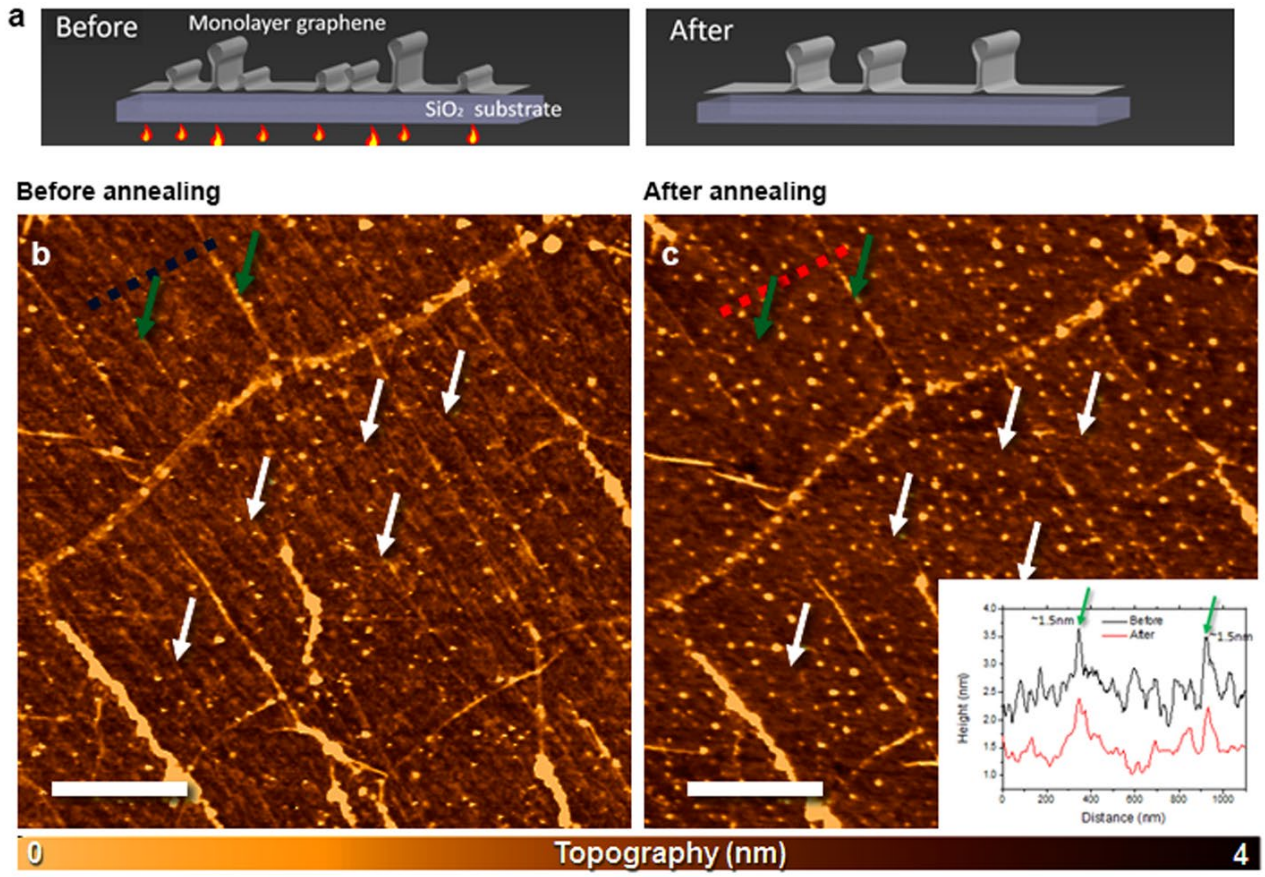

Figure 1 The thermal annealing effect on graphene wrinkles (a) The scheme for the monolayer graphene under thermal annealing, short wrinkles are removed while long wrinkles are stable. (b, c) The AFM topographic images for the same position of monolayer graphene sample, before and after annealing. The long wrinkles (e.g., green arrows marked) over 1.5 nm height are stable during annealing, and short wrinkles (e.g., white arrows marked) less than critical length are removed by thermal annealing. The inset of (c) shows the height profiles for the dashed line positions of AFM images in (b) and (c), black and red lines are before and after annealing, respectively. Scale bars=1μm.

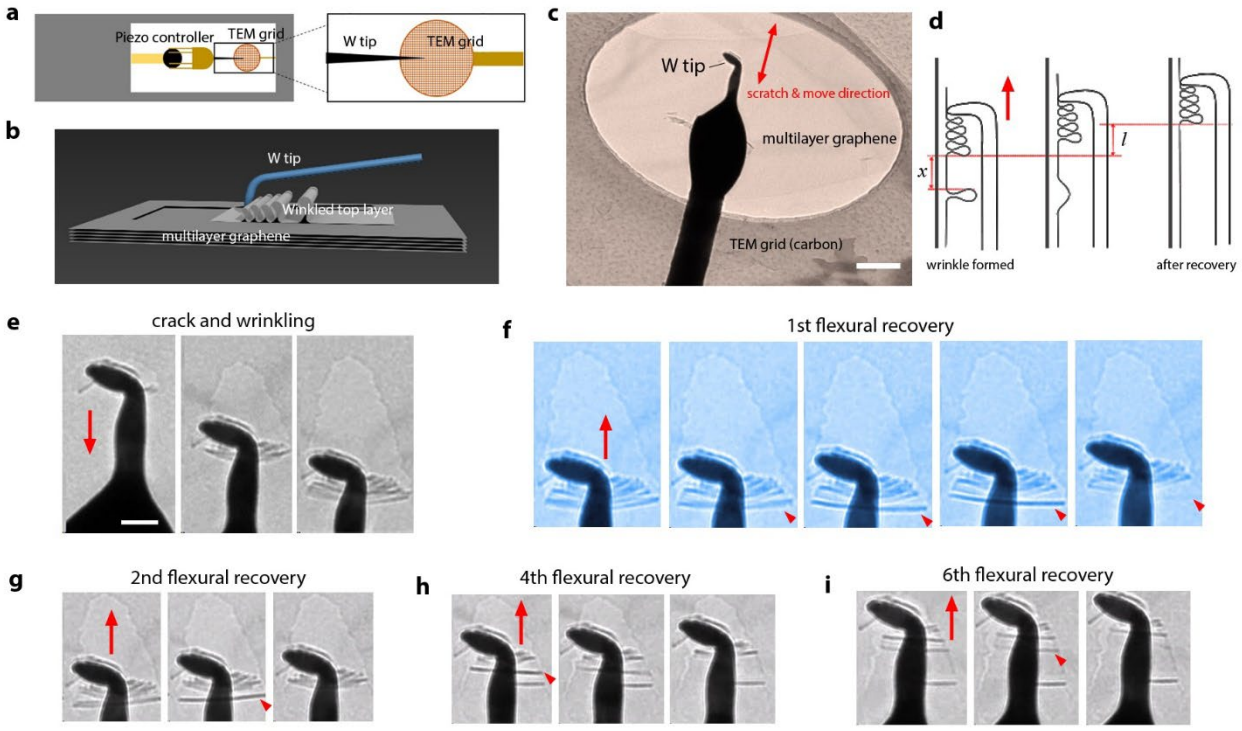

Figure 2. The *in situ* TEM wrinkling/dewrinkling tests on supported monolayer graphene. (a) Scheme for the *in situ* TEM setup. (b) Scheme for the exfoliation, wrinkling and manipulation on the surface top layer of graphene. (c) TEM image of the suspended multilayer flake and W tip, red arrow shows the tip moving direction, scale bar 100 nm. (d) Sequential scheme for the recovery flexural test and nomenclatures. (e) Sequential TEM micrographs for the cracking and wrinkle formation, scale bar 30 nm and following TEM images (f)-(i) at the same magnification. (f)-(i) Serial TEM micrographs show the recovery flexural tests for the 1st, 2nd, 4th and 6th times, respectively; the red arrows mark the tip moving directions; and the red triangles highlight the specified wrinkles under testing.

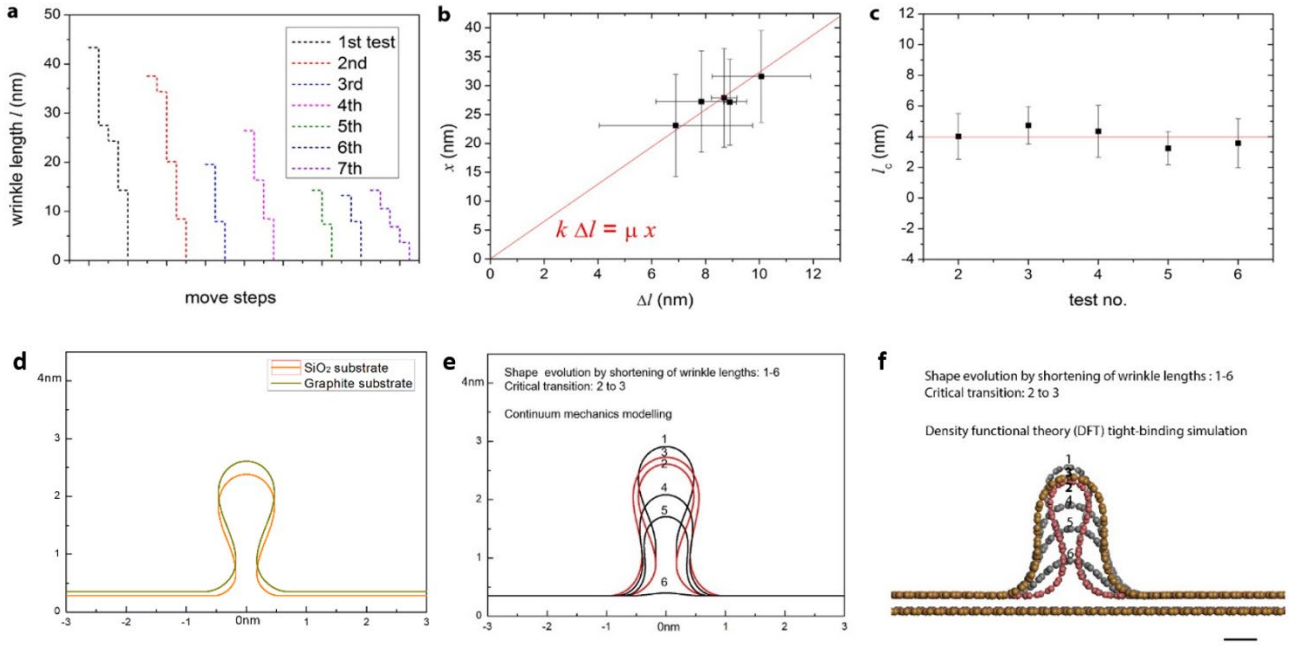

Figure 3. The results of TEM tests and wrinkling behaviour of monolayer graphene. (a) The stick-slip motion (wrinkle lengths) for each test. (b) Linear relationship between the change step of the wrinkle lengths (Δl) and sliding contact area (x). (c) The measured critical wrinkle lengths (after subtraction of the last move of the W tip). (d) The continuum mechanics models of critical wrinkle states on graphite and SiO_2 substrates. (e) The continuum mechanics models for the wrinkles at different lengths (length shrinking from state 1 towards state 6), unclip critical transition between state 2 and state 3. (f) The DFTB simulation results for the monolayer graphene wrinkles at different lengths (length shrinking from state 1 towards state 6) and the unclip critical transition between state 2 and state 3 (scale bar 0.5 nm).

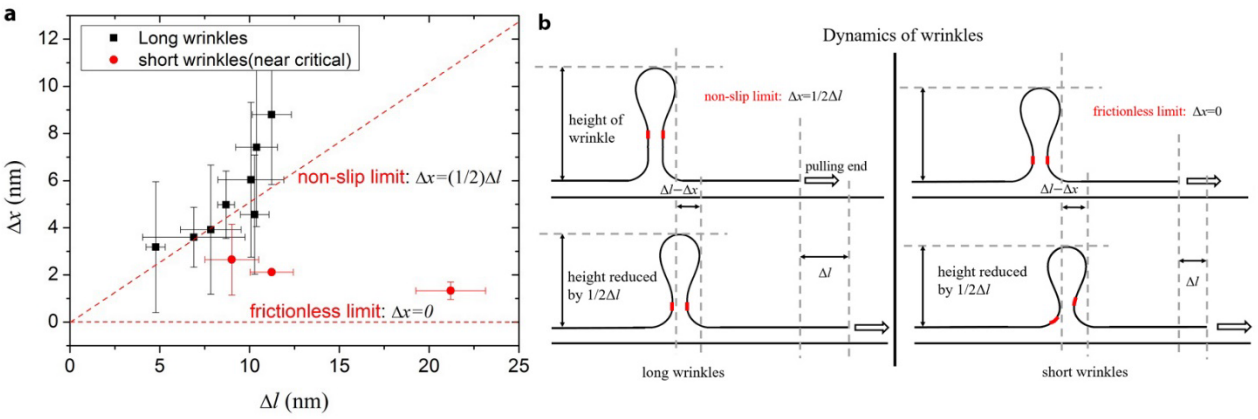

Figure 4. The experimental dynamics of the wrinkle position and lengths. (a) The experimental relationship between the length change and position change. The oblique and horizontal lines represent the non-slip limit and frictionless limit, respectively. (b) The schematics for the wrinkle dynamics in two limit cases (left and right). The red sections on the wrinkles labelled the same position on the wrinkle before and after pulling, respectively.